CHINESE OPTICS LETTERS

Vol. 21, No. 1 | January 2023

Photo-reconfigurable and electrically switchable spatial terahertz wave modulator [Invited]

Hongguan Yu (于宏冠), Huacai Wang (王华才), Zhixiong Shen (沈志雄), Shina Tao (陶师娜), Shijun Ge (葛士军)*, and Wei Hu (胡 伟)**

College of Engineering and Applied Sciences, Nanjing University, Nanjing 210093, China

*Corresponding author: geshijun@nju.edu.cn

**Corresponding author: huwei@nju.edu.cn

Received August 13, 2022 | Accepted September 30, 2022 | Posted Online October 27, 2022

Spatial terahertz wave modulators that can arbitrarily tailor the electromagnetic wavefront are in high demand in nondestructive inspections and high-capacity wireless communications. Here, we propose a liquid crystal integrated metadevice. It modulates the terahertz wave based on the adjustable electromagnetically induced transparency analog when spatially changing the environmental refractive index. The functions of the device can be arbitrarily programmed via photo-reorienting the directors of liquid crystals with a digital micromirror device-based exposing system. The thin liquid crystal layer can be further driven by an electric field, and thus the function can be rapidly switched. Amplitude modulation and the lens effect are demonstrated with modulation depths over 50% at 0.94 THz.

Keywords: terahertz; spatial terahertz wave modulator; metasurface.

DOI: 10.3788/COL202321.010002

1. Introduction

Terahertz (THz) waves, whose frequency is typically in the range between 0.1 and 10 THz, are of low photon energy and high penetration to nonpolar materials, and are widely used in biomedicine, security checks, and nondestructive evaluation[1–3]. Its higher frequency compared to microwave makes it promising in radar detection and 6G wireless communication as well[4]. To realize the above applications, functional devices are indispensable. Due to their exotic electromagnetic property and flexible design, metasurfaces have been widely explored in THz functional devices, such as planar polarizers, absorbers, and metalenses[5–7]. By designing metasurface dynamic phase and geometric phase, achromatic and spherical aberration-corrected metalenses have been realized[8,9]. The function of the metasurface is fixed once fabricated. To solve this problem, various tunable materials such as graphene[10], vanadium dioxide[11], and PIN diodes[12] have been adopted to achieve dynamic and reconfigurable functions. Liquid crystals (LCs) especially possess broadband birefringence and are responsive to multiple external fields, making them very suitable for active THz metadevices[13].

The switching of the above devices is still restricted to certain functionalities; dynamic and free manipulation of THz waves has kept being an urgent pursuit. Spatial THz wave modulators (STMs) can arbitrarily and dynamically manipulate the amplitude, phase, and polarization of electromagnetic waves[14–16], therefore supplying a way for THz manipulation with programming functionalities. A digital micromirror device (DMD) is utilized to spatially program the laser to locally control the photogenerated carriers of high-resistance silicon or graphene and alter the THz wave transmission or reflection accordingly[17,18]. These light-driven STMs have been successfully utilized in compressive imaging[19], holographic projection[20], and zoom lenses[21]. However, the resolution is limited by the cross talk between adjacent pixels due to the diffusion of photogenerated carriers. Electrically driven STMs have also been demonstrated by using feed networks and field programmable gate array (FPGA) to discretely control the separate units[22,23]. According to the resonance variation of the metasurface induced by the bias, the phase or amplitude of each unit can be dynamically regulated. This technique has great potential in radar detection and 6G wireless communication[24]. Scaling up the pixel amount is necessary to realize complicated functions. Moreover, continuous energy supply is required to maintain the function for all of the above STM techniques. Nonvolatile memorable STM has been much less documented. Very recently, the first programmable memory metasurface with serial pixel control was demonstrated based on the hysteresis characteristics of vanadium dioxide. After external stimuli are removed, the function can still be stored for over 10 h[25].

In this Letter, a nonvolatile STM of photo-reconfigurability and electrical switchability is proposed. It is an LC-integrated

metasurface and works on the shift of electromagnetically induced transparency (EIT) analog caused by the variation of the environmental refractive index. Two parallel and polarization-sensitive photoalignment layers are adopted to control the local orientation of LCs in each pixel. The orientation of LCs can be rewritten by recording another image generated by the DMD; thereby the amplitude of THz wavefront can be freely programmed in a reconfigurable manner. The photo-imprinted functions can be rapidly switched off by applying a certain bias. It supplies a reconfigurable and high-fidelity holographic platform for THz imaging and sensing, and may inspire various advanced applications.

2. Principle and Design

Figure 1(a) illustrates the configuration of the LC-integrated metadevice. Two 500-μm-thick fused silica layers are used as the superstrate and substrate, respectively. The superstrate is covered by a few-layer graphene electrode, while the substrate is covered by a specially designed metasurface. Both of them are coated with a photoalignment layer, and then the LC is sandwiched to form the device.

The fabricated metasurface is revealed in Fig. 1(b). Detailed dimensions of the repeated units are labeled in the inset. For such a lying "H" array, a strong broad dipole resonance occurs. When the middle slit is displaced laterally, i.e. $d_1 \neq d_3$, the symmetry broken further introduces a nonradiative quadrupole resonance. We optimize the geometric parameters of the antenna by finite difference time domain (FDTD) method to make the two resonances occur at the same frequency (1.07 THz). The reflection spectrum of the metasurface for x-incident polarization is shown in Fig. 2(a). As expected, a high Q-factor plasmonic EIT analog[26] is obtained with a peak at 1.07 THz. Figure 2(b) exhibits a narrow resonant transmission dip at the same frequency.

Lumerical FDTD Solutions is adopted to simulate the performance of the metasurface. The conductivity of Au and the refractive index of the substrate are set as 4.09×10^7 S/m and 1.92, respectively. The x–y plane and z direction are set as the periodic boundary condition and perfectly matched layer, respectively. Figure 2(c) reveals the distribution of the electromagnetic field. The dipole and quadrupole resonances are excited simultaneously; moreover, the energy is localized in the unit. Figure 2(d) shows that antiparallel-induced surface currents are generated and accumulate along the y direction, causing destructive interference. Both the localized electric field and induced surface currents are along the y axis; therefore, the EIT analog is sensitive to the refractive index change corresponding to this direction.

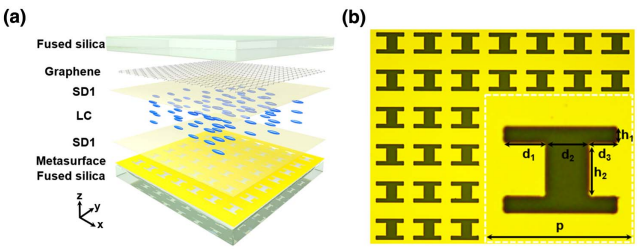

Fig. 1. (a) Schematic illustration of the LC-integrated metasurface; (b) micrograph of the designed metasurface. Inset shows the detailed dimensions: p = 110 μm; d_1 = d_2 = 30 μm; d_3 = 20 μm; h_1 = 10 μm; and h_2 = 40 μm.

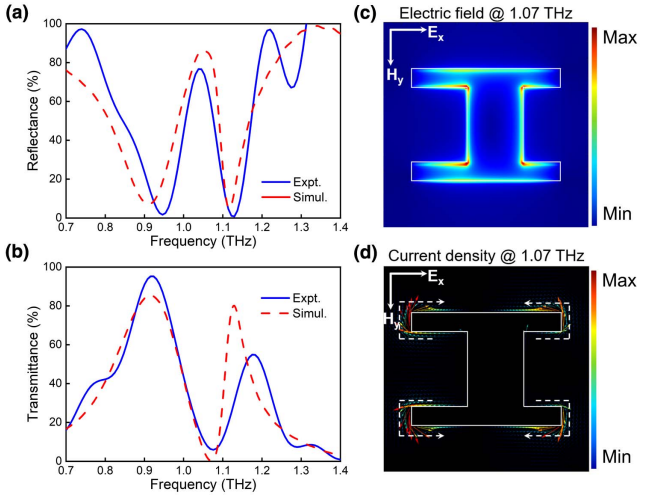

Fig. 2. (a) Reflection and (b) transmission spectra of the metasurface for x-polarized incidence; (c) electric field and (d) current density distribution of a single unit at 1.07 THz. The white dashed arrows in (d) depict the directions of induced surface currents.

3. Simulation and Experiment

The Au pattern, whose thickness is 200 nm, is fabricated by standard photolithography, electron beam evaporation, and the lift-off process. Sulfonic azo dye (SD1, DIC Co., Japan) is spin-coated as the photoalignment layer. SD1 molecules tend to reorient perpendicularly to the polarization direction of incident 405 nm LED blue light, and then guide the LC directors toward the same direction. It exhibits excellent photo-rewritability, and only the polarization direction of the last exposure is recorded[27]. The superstrate and substrate are separated by 50-μm-thick Mylar and exposed simultaneously to form a homogeneous cell. Finally, a high birefringent nematic LC NJU-LDN-4[28] ($\Delta n > 0.30$ in the measured THz range) is capillary-infiltrated. Since the phase delay induced by the LC layer is far from the half-wave condition, the diffraction effect is negligible, and the LC here only acts as a refractive-index variable environmental medium to change the resonance of the metasurface. The orientation of LCs is adjusted by tuning the direction of a polarizer, and the exposure is carried out with a saturated voltage of 20 V to eliminate the influence of the LC.

We use a THz time-domain spectrometer (TAS7500SP; Advantest Corporation, Tokyo, Japan) to characterize the sample. Figure 3 shows the dependencies of reflection and transmission on the orientation of LC θ. A 50-μm-thick LC cell is used as

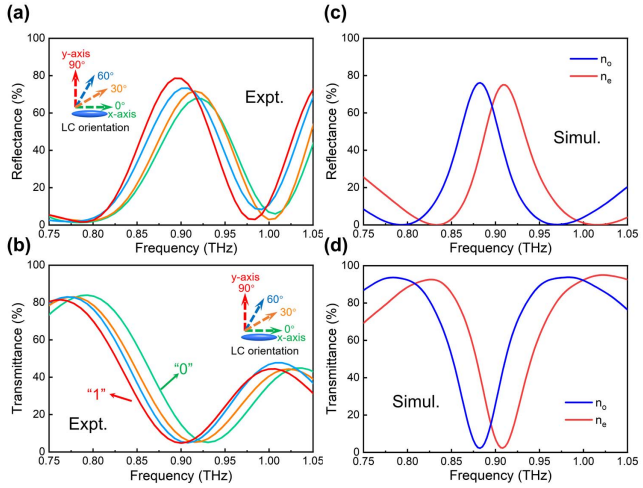

Fig. 3. Measured (a) reflection and (b) transmission at $\theta = 0°$, 30°, 60°, and 90°, respectively; simulated (c) reflection and (d) transmission when the easy axis of the LC is along the *x* axis (red curve) and *y* axis (blue curve), respectively.

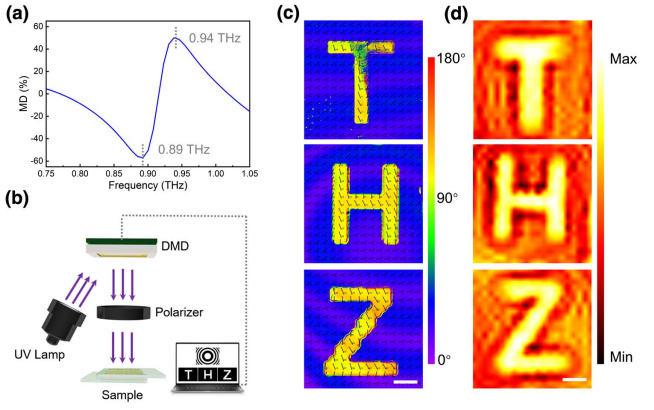

Fig. 4. (a) Schematic diagram of the DMD-based polarization exposing setup; (b) measured dependency of the transmission modulation depth on the frequency; (c) measured LC director distributions of the STM when outputting "T", "H," and "Z;" (d) amplitude modulations of the STM when outputting "T", "H," and "Z" at 0.94 THz. All scale bars indicate 1 mm.

the reference for the test. When the easy axis moves from along the *x* axis to along the *y* axis, the reflection peak shifts from 0.923 to 0.892 THz as a result of the refractive index change, as shown in Fig. 3(a). Figure 3(b) reveals that the transmission dip ($Q = 8.1$) shifted from 0.926 to 0.894 THz, accordingly. In the FDTD simulation, we set the anisotropy of the LC as $n_o = 1.6 + 0.01i$ and $n_e = 1.9 + 0.005i$. The simulation suggests similar spectral shifts compared to the experiments. The LC rotation caused spectral shifts are simulated by changing the optical axis of the birefringent media. The reflection peak shifts from 0.908 to 0.885 THz, and the transmission dip ($Q = 15.8$) shifts from 0.910 to 0.881 THz. Compared to the simulations, the wide resonance and lower *Q* factor in experiments are derived from the loss introduced by LCs. The lower intensity of the high-frequency transmission peak is due to the frequency mismatch of the dipole resonance and the nonradiative quadrupole resonance in the real condition caused by fabrication deviations.

The orientation change of the LCs induces a significant transmission variation at certain frequencies. Herein, we define the orientations of the LCs along the *x* axis and *y* axis as 0 and 1 states, respectively. The corresponding modulation depth (MD) is depicted as MD = $(T_1 - T_0)/(T_1 + T_0)$. As shown in Fig. 4(a), the MD exceeds 50% at 0.94 and 0.89 THz, suggesting that the device is usable at multiple wavelengths. By spatially encoding the orthogonal LC orientations to the same LC-integrated metadevice, STM can be realized. As presented in Fig. 4(b), we use a DMD consisting of 1024 × 768 micromirrors to generate the objective pattern and then project it to the cell through a nanowire-grid polarizer[29]. This technique enables arbitrary wavefront control on the THz wave.

For demonstration, the letters "T", "H," and "Z" are subsequently recorded for the same sample. As mentioned above, the rewriting is carried out under saturated voltages. The sample is erased by a uniform linearly polarized light for 2 min first, and then exposed under the DMD-based exposing system to record the objective pattern with a 90° rotated polarizer for another 2 min. Images in Fig. 4(c) indicate that the LC orientations inside the letters are perpendicular to those outside. The measured director distributions are consistent with the designs. We further characterize the spatial amplitude modulations of the STM using a THz near-field scanning system (TP800, Terahertz Photonics Co. Ltd., China). When the *x*-polarized THz wave is incident on the sample, patterns consistent with the letters "T", "H," and "Z" are captured accordingly, as shown in Fig. 4(d). It vividly verifies the spatial amplitude modulation functionality of the STM.

Besides information displays, the proposed STM enables various diffractive optics as well. Here, we design a Fresnel zone plate with focal length of 6 mm. We binarize the transfer function $T_{\mathrm{FZP}} = \exp(-i\pi r^2/\lambda f)$ to obtain the diffractive pattern for the Fresnel zone plate. Figure 5(a) shows the LC orientations of the photopatterned sample. The LC directors are perpendicular to each other in the odd and even bands of the Fresnel zone plate. Figure 5(b) exhibits the intensity distribution at the focal plane. The THz wave is focused in the far field, revealing the good focusing function of the element. Meanwhile, with a 20 V saturated bias applied, all LCs orient along the *z* axis, the lens function is switched off, and a transmitted Gaussian beam is recorded, as shown in Fig. 5(c).

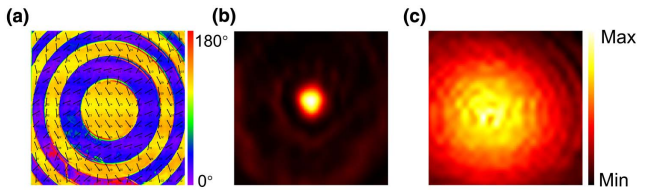

Fig. 5. Fresnel zone plate with $f = 6$ mm. (a) Measured LC distribution; intensity distribution at the focal plane when applying voltages of (b) 0 V and (c) 20 V, respectively.

4. Discussion

THz amplitude modulation is realized by programming the LC orientation of the LC-integrated metadevice. The excellent flexibility and high resolution of the generated pattern lead to an arbitrary STM capability. The function is nonvolatile, since the LC orientation is stable until the next exposure is carried out. The device is also photo-reconfigurable. Besides the functions presented, other functions such as beam steering and specific THz field generation can be reasonably expected. Compared to the wavefront modulation based on a pure photo-patterned LC, the cell thickness of the proposed STM is much smaller, resulting in lower driven voltage and faster response. Since the reflection spectrum is compensatory to the transmission, the proposed STM can work in reflection mode as well. The LC-integrated metadevice is ultrathin and compact. Two different modulation ways are involved in this work: photo-reconfiguration and electrical switch. The speed of the previous one is restricted by the responsiveness of SD1, which is typically in minutes scale and could be drastically improved by increasing the power of the pump source or introducing a more sensitive photoalignment agent. The electrical switching speed is dependent on the thickness and the intrinsic properties of the LCs. It is commonly in milliseconds and can be improved by reducing the cell thickness or adopting fast response dual-frequency LCs or ferroelectric LCs. It supplies a nonvolatile, reconfigurable, and transflective technique for spatial THz wave modulation.

5. Conclusion

We proposed and demonstrated a photo-reconfigurable and electrically switchable STM. Through photopatterning LCs to control the environmental refractive index, arbitrary and dynamic spatial THz modulation is realized due to the corresponding peak shift of the EIT analog. By this means, the letters "T", "H," and "Z" and the Fresnel zone plate are presented with a modulation depth of over 50%. The function can be rapidly switched off and on by applying a proper voltage to the cell. The design is compact, nonvolatile, and reconfigurable, exhibiting great potential in THz imaging, sensing, and monitoring.

Acknowledgement

This work was supported by the National Natural Science Foundation of China (NSFC) (Nos. 62035008, 62105143, and 61922038), the Natural Science Foundation of Jiangsu Province (No. BK20210179), and the Fundamental Research Funds for the Central Universities (No. 021314380189).

References

1. A. Gong, Y. Qiu, X. Chen, Z. Zhao, L. Xia, and Y. Shao, "Biomedical applications of terahertz technology," Appl. Spectrosc. Rev. **55**, 418 (2019).
2. K. B. Cooper, R. J. Dengler, N. Llombart, B. Thomas, G. Chattopadhyay, and P. H. Siegel, "THz imaging radar for standoff personnel screening," IEEE Trans. Terahertz Sci. Technol. **1**, 169 (2011).
3. R. I. Stantchev, B. Q. Sun, S. M. Hornett, P. A. Hobson, G. M. Gibson, M. J. Padgett, and E. Hendry, "Noninvasive, near-field terahertz imaging of hidden objects using a single-pixel detector," Sci. Adv. **2**, e1600190 (2016).
4. T. Nagatsuma, G. Ducournau, and C. C. Renaud, "Advances in terahertz communications accelerated by photonics," Nat. Photonics **10**, 371 (2016).
5. N. K. Grady, J. E. Heyes, D. R. Chowdhury, Y. Zeng, M. T. Reiten, A. K. Azad, A. J. Taylor, D. A. R. Dalvit, and H. Chen, "Terahertz metamaterials for linear polarization conversion and anomalous refraction," Science **340**, 1304 (2013).
6. G. Isić, B. Vasić, D. C. Zografopoulos, R. Beccherelli, and R. Gajić, "Electrically tunable critically coupled terahertz metamaterial absorber based on nematic liquid crystals," Phys. Rev. Appl. **3**, 064007 (2015).
7. X. Zang, W. Xu, M. Gu, B. Yao, L. Chen, Y. Peng, J. Xie, A. V. Balakin, A. P. Shkurinov, Y. Zhu, and S. Zhuang, "Polarization-insensitive metalens with extended focal depth and longitudinal high-tolerance imaging," Adv. Opt. Mater. **8**, 1901342 (2019).
8. Q. Cheng, M. Ma, D. Yu, Z. Shen, J. Xie, J. Wang, N. Xu, H. Guo, W. Hu, S. Wang, T. Li, and S. Zhuang, "Broadband achromatic metalens in terahertz regime," Sci. Bull. **64**, 1525 (2019).
9. S. Zhou, K. Xi, S. Zhuang, and Q. Cheng, "Spherical aberration-corrected metalens for polarization multiplexed imaging," Nanomaterials **11**, 2774 (2021).
10. X. Chen, Z. Tian, Y. Lu, Y. Xu, X. Zhang, C. Ouyang, J. Gu, J. Han, and W. Zhang, "Electrically tunable perfect terahertz absorber based on a graphene salisbury screen hybrid metasurface," Adv. Opt. Mater. **8**, 1900660 (2019).
11. J. Shabanpour, S. Beyraghi, and A. Cheldavi, "Ultrafast reprogrammable multifunctional vanadium-dioxide-assisted metasurface for dynamic THz wavefront engineering," Sci. Rep. **10**, 8950 (2020).
12. Q. Ma, G. Bai, H. Jing, C. Yang, L. Li, and T. J. Cui, "Smart metasurface with self-adaptively reprogrammable functions," Light Sci. Appl. **8**, 98 (2019).
13. Z. Shen, S. Zhou, X. Li, S. Ge, P. Chen, W. Hu, and Y. Lu, "Liquid crystal integrated metalens with tunable chromatic aberration," Adv. Photonics. **2**, 036002 (2020).
14. W. Chan, H. Chen, A. Taylor, I. Brener, M. J. Cich, and D. M. Mittleman, "A spatial light modulator for terahertz beams," Appl. Phys. Lett. **94**, 213511 (2009).
15. C. Liu, F. Yang, X. Fu, J. Wu, L. Zhang, J. Yang, and T. Cui, "Programmable manipulations of terahertz beams by transmissive digital coding metasurfaces based on liquid crystals," Adv. Opt. Mater. **9**, 2100932 (2021).
16. X. Bai, F. Kong, Y. Sun, G. Wang, J. Qian, X. Li, A. Cao, C. He, X. Liang, R. Jin, and W. Zhu, "High-efficiency transmissive programmable metasurface for multimode OAM generation," Adv. Opt. Mater. **8**, 2000570 (2020).
17. D. Shrekenhamer, C. M. Watts, and W. J. Padilla, "Terahertz single pixel imaging with an optically controlled dynamic spatial light modulator," Opt. Express. **21**, 12507 (2013).
18. Q. Wen, W. Tian, Q. Mao, Z. Chen, W. Liu, Q. Yang, M. Sanderson, and H. Zhang, "Graphene based all-optical spatial terahertz modulator," Sci. Rep. **4**, 7409 (2014).
19. S. M. Hornett, R. I. Stantchev, M. Z. Vardaki, C. Beckerleg, and E. Hendry, "Subwavelength terahertz imaging of graphene photoconductivity," Nano Lett. **16**, 7019 (2016).
20. Z. Xie, X. Wang, J. Ye, S. Feng, W. Sun, T. Akalin, and Y. Zhang, "Spatial terahertz modulator," Sci. Rep. **3**, 3347 (2013).
21. J. Guo, T. Wang, H. Zhao, X. Wang, S. Feng, P. Han, W. Sun, J. Ye, G. Situ, H. T. Chen, and Y. Zhang, "Reconfigurable terahertz metasurface pure phase holograms," Adv. Opt. Mater. **7**, 1801696 (2019).
22. J. Wu, Z. Shen, S. Ge, B. Chen, Z. Shen, T. Wang, C. Zhang, W. Hu, K. Fan, W. Padilla, Y. Lu, B. Jin, J. Chen, and P. Wu, "Liquid crystal programmable metasurface for terahertz beam steering," Appl. Phys. Lett. **116**, 131104 (2020).
23. W. Li, X. Hu, J. Wu, K. Fan, B. Chen, C. Zhang, W. Hu, X. Cao, B. Jin, Y. Lu, J. Chen, and P. Wu, "Dual-color terahertz spatial light modulator for single-pixel imaging," Light Sci. Appl. **11**, 191 (2022).
24. X. Fu, F. Yang, C. Liu, X. Wu, and T. Cui, "Terahertz beam steering technologies: from phased arrays to field-programmable metasurfaces," Adv. Opt. Mater. **8**, 1900628 (2019).
25. B. Chen, J. Wu, W. Li, C. Zhang, K. Fan, Q. Xue, Y. Chi, Q. Wen, B. Jin, J. Chen, and P. Wu, "Programmable terahertz metamaterials with non-volatile memory," Laser Photonics Rev. **16**, 2100472 (2022).

26. N. Liu, T. Weiss, M. Mesch, L. Langguth, U. Eigenthaler, M. Hirscher, C. Sönnichsen, and H. Giessen, "Planar metamaterial analogue of electromagnetically induced transparency for plasmonic sensing," Nano Lett. **10**, 1103 (2009).
27. J. Sun, A. K. Srivastava, L. Wang, V. G. Chigrinov, and H. S. Kwok, "Optically tunable and rewritable diffraction grating with photoaligned liquid crystals," Opt. Lett. **38**, 2342 (2013).
28. L. Wang, X. Lin, X. Liang, J. Wu, W. Hu, Z. Zheng, B. Jin, Y. Qin, and Y. Lu, "Large birefringence liquid crystal material in terahertz range," Opt. Mater. Express. **2**, 1314 (2012).
29. H. Wu, W. Hu, H. Hu, X. Lin, G. Zhu, J. W. Choi, V. Chigrinov, and Y. Q. Lu, "Arbitrary photo-patterning in liquid crystal alignments using DMD based lithography system," Opt. Express **20**, 16684 (2012).